applied sciences

MDPI

Article

Research on a 3D Seismic Horizon Automatic-Tracking Method Based on Corrugated Global Diffusion

Mingjun Su [1,*], Feng Qian [2], Shengkai Cui [2], Cheng Yuan [1] and Xiangli Cui [1]

[1] Research Institute of Petroleum Exploration & Development-Northwest, Lanzhou 730020, China
[2] School of Information and Communication Engineering, University of Electronic Science and Technology of China, Chengdu 611731, China
* Correspondence: sumj@petrochina.com.cn

Abstract: The core challenges to automatic full-horizon tracking are how to establish a potential local connection relationship between the horizon points, conduct accurate global diffusion in a three-dimensional space, and finally, how to form a complex horizon surface. The existing attribute-based horizon-tracking methods based on waveform similarity, dip guidance, and RGT (relative geological time) can not solve the problems of local connection and global diffusion at the same time. In view of this challenge, this paper proposes an automatic 3D seismic horizon-tracking method based on global corrugated diffusion, which can completely integrate local connection and global diffusion so that all horizons in the whole data volume can be interpreted simultaneously. For the problem of local horizon-point connection, this paper uses the correlation between seismic trace pairs based on DTW (dynamic time warping) correlation to mine the connection mode between horizon points. For the global diffusion problem, this paper proposes the realization of global modeling based on the relationship between seismic samples, constructing a complex 3D horizon through a central ripple-diffusion process. The example shows that the horizon tracked by this method well reflects the original stratum occurrence and stratum-contact relationship, retains the structural details, accurately reflects the structural shape, and realizes automatic tracking across faults.

Keywords: automatic full-horizon tracking; dynamic time planning; corrugated global diffusion; 3D seismic data; correlation coefficients

Citation: Su, M.; Qian, F.; Cui, S.; Yuan, C.; Cui, X. Research on a 3D Seismic Horizon Automatic-Tracking Method Based on Corrugated Global Diffusion. *Appl. Sci.* **2023**, *13*, 6155. https://doi.org/10.3390/app13106155

Academic Editor: Giuseppe Lacidogna

Received: 2 March 2023
Revised: 23 April 2023
Accepted: 24 April 2023
Published: 17 May 2023

1. Introduction

At present, oil and natural gas are the most important sources of energy for human survival, and it is difficult to replace these with other energy sources for a long period of time. In order to exploit oil and gas reservoirs, it is necessary to understand the subsurface structure, which is inseparable from seismic data interpretation. Good seismic data interpretation results are conducive to the accurate development and utilization of underground complex oil and gas reservoirs. Horizon tracking is the process of identifying horizons in 3D seismic images and distinguishing them from each other. It is the most fundamental and important part of seismic interpretation work [1,2] and the accuracy of the tracking results directly affect the quality of the subsequent seismic image interpretation results. Traditionally, geologists have manually labeled horizons on 2D sections, which requires manual tracking for each section. With the advent and development of high-precision, fully digital acquisition systems, the amount of manual tracking work has become extremely large, seriously affecting the efficiency of seismic interpretation. Integrating artificial intelligence, image-processing techniques, and other methods to achieve fully automatic horizon tracking using 3D seismic images has become a hot research topic. The core challenge of automatic full-horizon tracking is how to establish the relationship between horizon points and accurately diffuse them in 3D space to finally form complex horizon bodies.

In order to address these core challenges, people have made various attempts, which can be specifically divided into three categories: horizon tracking methods based on waveform similarity [3], on dip, or on RGT. The former directly processes horizon waveforms in the time domain. The most typical work is the waveform similarity algorithm based on the cost function, as proposed by Pauget et al. [4], to achieve automatic horizon tracking. Horizon-tracking methods based on dip map waveform similarity into the attribute of dip, and then use dip to indicate the horizon extension direction. One typically cited work is the seismic dip-driven method by de Groot et al. [5], which recognizes the horizon under the guidance of dip. As for horizon-tracking methods based on RGT, these use an extension of the dip method and represent this to another new domain, the instantaneous phase domain, which is essentially another attribute. The typically cited work in this area includes Star et al. [6,7], Wu et al. [8], and Geng et al. [9], who applied seismic instantaneous-phase-unraveling methods to achieve automatic horizon tracking. In practical applications, noise interference and complex region waveform distortion pose serious challenges to the assumption of the same horizon waveform similarity, leading to incorrect tracking results. In order to overcome dependence on human assumptions, people have developed AI-based methods that do not require any assumptions and hope to track the horizon in a data-driven manner. For example, Harrigan et al. [10] applied artificial neural networks to horizon tracking; Borgos et al. [11] applied clustering algorithms to horizon tracking, which was mainly based on the statistical characteristics of horizon waveforms. Tschannen et al. [12] used supervised deep learning, and Shi et al. [13] adopted unsupervised deep learning methods to track horizon positions.

Although existing methods have, to some extent, solved the core challenges of horizon-position tracking and achieved certain results, there are still the following problems: (1) most of the current research focuses on single-horizon tracking rather than full-horizon tracking and building horizon-position connections is more challenging for full-horizon tracking because the interference of waveforms in the time direction will intensify, while single-horizon tracking only needs to consider the matching of waveforms in adjacent traces; (2) waveform similarity measures only establish connections between local horizon position points, without considering the entire spatial diffusion problem. Moreover, similarity measures are directional, and local similarity measures cannot achieve optimal results globally; (3) RGT and inclination are not sufficiently precise, and there are often modeling errors in the mapping process, resulting in the inability to accurately indicate horizon extension direction.

Given the limitations of the existing methods and the severe challenges in tracking horizons using 3D seismic data, this paper proposes a novel automatic horizon-tracking method for 3D seismic data based on the DTW (dynamic time warping) algorithm [14–17]. The method is mainly divided into two steps: (1) the establishment of a local connection relationship by utilizing the correlation between seismic traces based on DTW; adjacent traces are connected to form a trace set, as shown in Figure 1; (2) the establishment of a global diffusion model based on the relationship between seismic samples, where a global model is established, and the center trace set is expanded outward to obtain a clear optimal model, finally realizing automatic horizon tracking by using 3D seismic data.

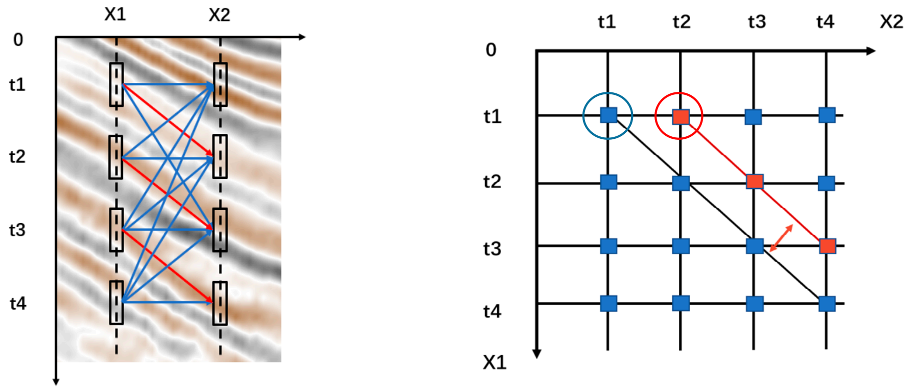

(**a**) (**b**)

Figure 1. Calculation diagram of similarity coefficient matrix. (**a**) Two adjacent seismic channels: X1 and X2; (**b**) corresponding correlation coefficient grid.

2. Method

As stated above, the DTW-based waveform global diffusion auto-tracking algorithm can be divided into two stages for different processing objects, as follows.

2.1. Stage 1: Local Connection Algorithm Based on Dynamic Time Warping Algorithm

After sampling the original seismic data, a regularized sample space is obtained. In the sample space, the two neighboring seismic traces, X1 and X2, are selected, and the correlation between each point in X1 and each point in X2 is calculated. The arrows in Figure 1a represent the different connections, and the different matching relationships can be seen in Figure 1b. The blue squares inside the blue circles in Figure 1b represent the correlation value between the seed point of X1 at t1 and the seed point of X2 at t1, and the red squares inside the red circles represent the correlation value between the seed point of X1 at t1 and the seed point of X2 at t2. There are two lines in Figure 1b representing the different matching paths between the seed points contained in X1 and X2.

When searching for horizon positions, correspondences with high correlation coefficients are likely. When a set of high-probability correspondences is drawn as a segment, we get a "correlation comb", which connects multiple seismic reflection points. The dynamic time warping (DTW) algorithm is used to identify the best "correlation comb" with the highest correlation.

Dynamic time warping (DTW) algorithm: It describes the time correspondence between a test template and a reference template using a time regularization function W(n) that satisfies certain conditions (bounds limit, monotonicity limit, and continuity limit), solves for the regularization function that corresponds to the minimum accumulated distance when matching the two templates, and thus obtains the best path (best "correlation comb") between two points (Figure 2).

Figure 2a has no actual meaning in the *y*-axis, and the *x*-axis represents the sample points in the time series.

In Figure 2a, when comparing the similarity between the solid line and the dotted line time series, if time is kept consistent, point a of the solid waveform will correspond to point b′ of the dotted waveform, but in reality, point a of the solid line corresponds to point b of the dotted line. The DTW algorithm calculates the similarity between two time series by stretching and shortening the time series. The matching process is shown in Figure 2b, where the *y*-axis represents the solid line A of length Q in Figure 2a, and the *x*-axis represents the dotted line B of length C in Figure 2a, and each square represents the correlation between the i-th point of line A and the j-th point of line B. The optimal path from w1 to wk is found through DTW, and the result is shown by the solid dot set that forms the path, as shown in Figure 2b.

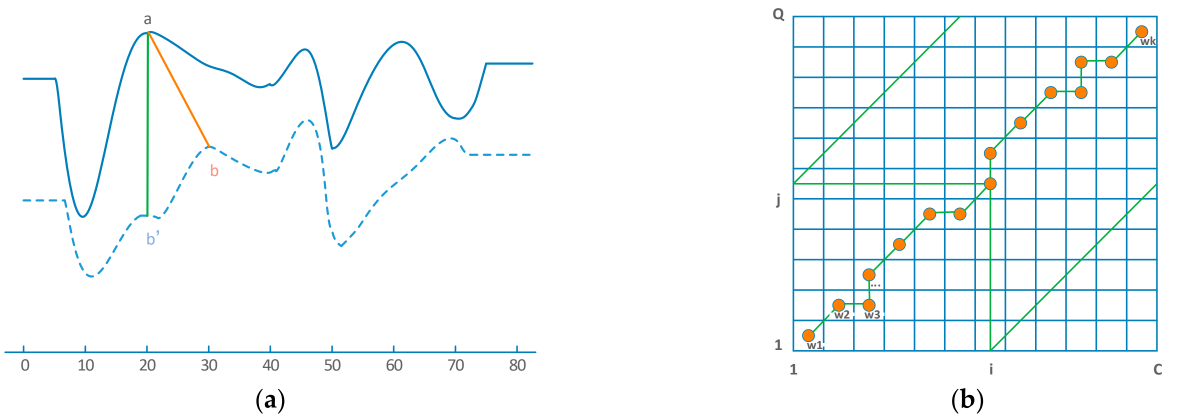

Figure 2. Schematic diagram of DTW technology. (**a**) Compare the similarity of the two time series; (**b**) DTW algorithm to solve the best "correlation coefficient comb".

It is worth noting that Figure 2b is a real example that calculates the similarity between two time series $Q =, q_2, \ldots, q_i, \ldots q_n$ and $C = c_1, c_2, \ldots, c_j, \ldots c_m$. The matrix element (i, j) in Figure 2b represents the similarity between two points q_i and c_j. By using the DTW algorithm, the best path between two points is obtained: w_1, w_2, w_3, $w_4 \ldots w_k$, as indicated by the orange dots in Figure 2b.

Figure 3a is a plot of the correlation coefficient calculated based on the actual seismic tracks (X1, X2). The yellow-green color represents the magnitude of the correlation between data points in the two tracks, with yellow indicating a high correlation and green indicating a low correlation. Figure 3b is the best path extracted from Figure 3a based on DTW, consisting of a large number of points, and its linear property is comparable to the w1 to wk path in Figure 2b, that is, the best "correlation comb" with maximum correlation.

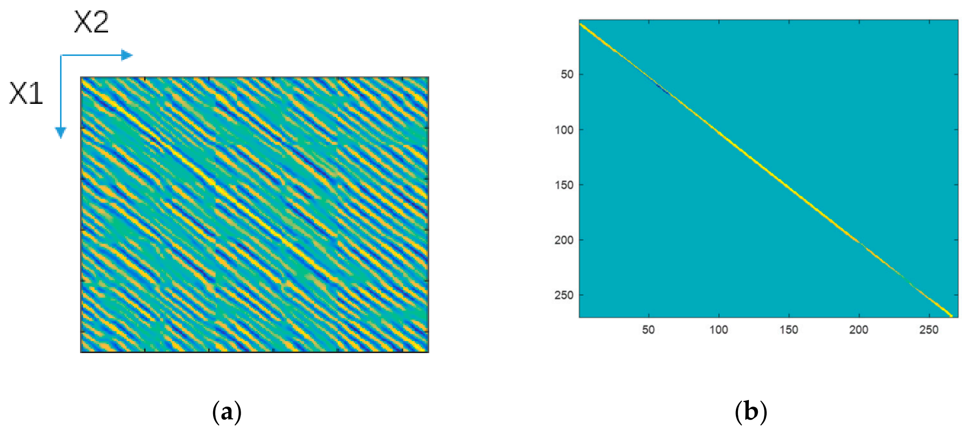

Figure 3. Schematic diagram of DTW extracting the best relevant segment. (**a**) Correlation coefficient diagram calculated from actual seismic channels; (**b**) the best correlation segment extracted by the DTW algorithm.

2.2. Stage 2: Ripple-Type Global Spatial Diffusion Method

After establishing the local connection between the horizon points based on DTW, we need to diffuse this connection throughout the entire field, thus forming the complex horizons in the entire field. The selection scheme for the seed tracks remains unchanged, and the middle track is selected as the seed track. In the first step, the seed track x (timeline $\times$ 1 $\times$ 1) is spread outward to a labeled matrix of size timeline $\times$ 3 $\times$ 3. The specific method is shown in Figure 4.

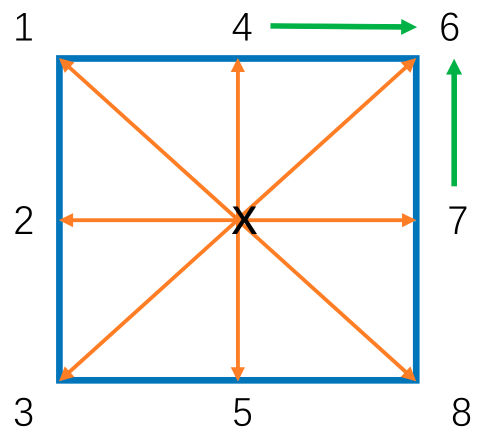

Figure 4. First diffusion diagram.

Set the central road as X, and transfer the label of X road to [1, 2, 3, 4, 5, 6, 7, 8] for a total of 8 data roads via the DTW algorithm. If there is a mapping horizon position between two adjacent roads, it means that each horizon position point on the surrounding 8 data roads can calculate 3 correlation coefficient values with the surrounding 3 roads. For example, a seed point marked as θ on the 6th road can calculate the correlation coefficient with the seismic roads 4, 7, and X.

The specific algorithm works as follows:

Step1: select point θ on X lane and choose 3 points around 8 lanes as the optional connection for this point; then, based on the optimal global correlation coefficient, choose the optimal connection group of the current point θ, forming a horizon surface. From this, obtain the optimal connection of all points on the X lane set.

Step 2: calculate the correlation coefficient value of each optimal connection, and label all groups in order of strongest to weakest correlation. This avoids labeling conflicts between two strata.

Step3: when selecting candidate points, according to the actual geological horizon attribute, the spatial positions of the same horizon label between two adjacent timeline traces are generally within ± 2, i.e., the inclination $\Omega \leq \arctan 2$. This is the spatial constraint added when performing DTW-based correlation coefficient calculations for actual seismic data. As shown in Figure 5, trace X contains a certain type of subpoint θ. If the horizon assignment work for θ is performed, then the mapping point of trace 1 is within 5 data points with a range of ± 2 units in the θ time axis co-ordinate. The correlation of a data segment containing a θ label position and a data segment of the same size containing one of the 5 points is obtained by DTW calculation.

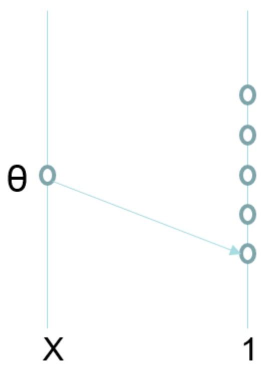

Figure 5. Space constraints.

Step 4: select 3 points with stronger correlation coefficients as alternative points. These 3 alternative points serve as the basis for the next step—the selection of the optimal connection path. Based on the optimal connection path, the optimal horizon position can be obtained, and the label is transferred to the optimal horizon position, thus completing the horizon tracking of a data point.

Once the first diffusion is completed, the second round of diffusion is performed. First, the labeling transfer direction is determined. If the first horizon labeling transfer work is mapped from the seed point in seismic road b to seismic road 3, the direction is shown (Figure 6).

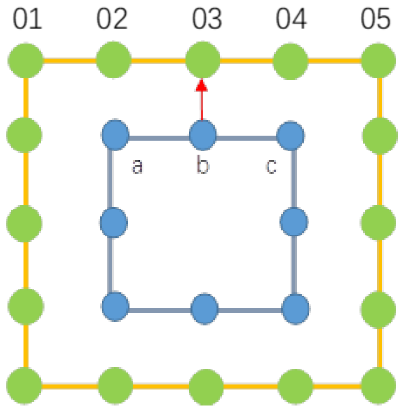

Figure 6. Label transfer direction.

The transfer relationship confirmed in Figure 7 is the labeling transfer process of a certain label from the b lane of the timeline $\times$ 3 $\times$ 3-labeled matrix to lane 3 of the timeline $\times$ 5 $\times$ 5 matrix. After the transfer road and mapping road are confirmed, the next step will be the selection of the diffusion window.

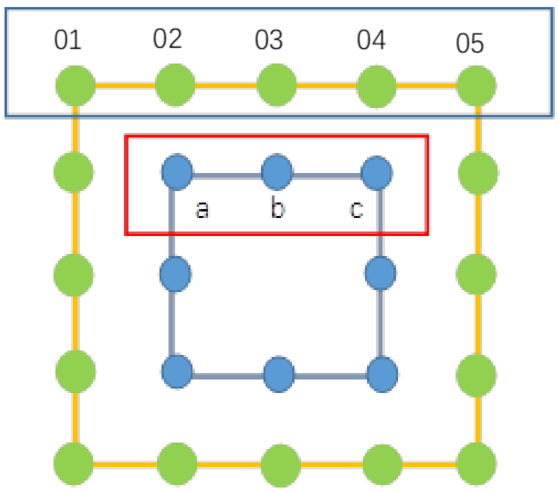

Figure 7. Selection of diffusion window.

As shown in Figure 7, select the two lanes on the left and right of the diffusion road (b road) as the diffusion window ([a, b, c]) and the two lanes on the left and right of the diffused road (3 roads) ([1, 2, 3, 4, 5]) as the diffused window. These two data windows are the dataset for the next step of DTW relevance calculation.

The next step is to select backup points. Once the diffusion window is confirmed, 3 backup points regarding the labeled horizon θ can be selected through the diffusion relationship. The diffusion relationship is shown in Figure 8.

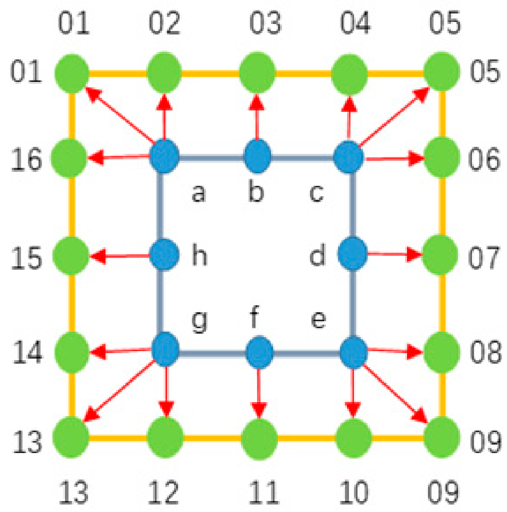

Figure 8. Diffusion relation.

The calculation of θ horizon is carried out by selecting the candidate points of the horizon according to the guiding relationship shown by the arrow in the Figure 5, with the [1, 2, 3, 4, 5] as the spreading window. The selection method is not much different from other DTW horizon-tracking algorithms. By calculating the partial dataset between road a and road 1 with respect to the θ horizon, 3 candidate points can be selected from among the 5 candidate points (as shown in Figure 5), and 15 candidate points can be obtained for the 5 datasets in the spreading window. Then, the next step is to calculate the correlation coefficient.

This step is also where the algorithm differs from other DTW-based horizon-tracking algorithms. To strengthen the association between the horizon points within the same horizon plane, this paper abandons the horizon propagation method (from single horizon to single horizon) and, instead, chooses to use it as a basis for the next processing step, which is the calculation of the correlation between the same horizon label within the expanding window between different data horizons.

The calculation relationship is shown in Figure 9.

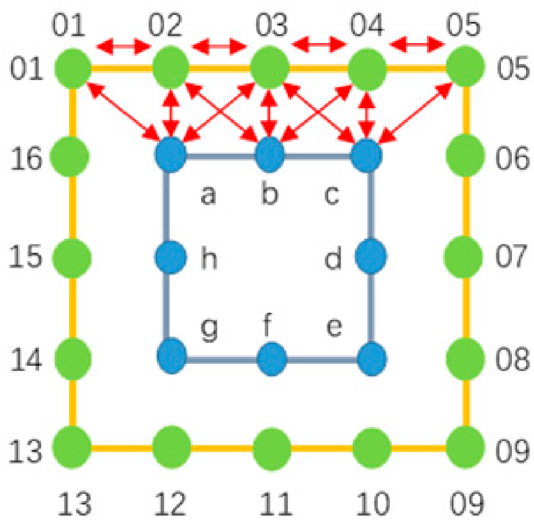

Figure 9. Correlation coefficient calculation.

According to the arrow direction shown in the above graph, after the inner and outer diffusion windows are determined, the correlation between horizons can be calculated according to Figure 9. In order to strengthen the correlation between horizon points during horizon diffusion, the range of the calculated data is expanded as much as possible when using the DTW algorithm to calculate the correlation of the time series. The increase in data calculation means an increase in the space and time costs required by the algorithm, but this also improves the accuracy of the calculation results.

According to the arrows indicated in Figure 9, there are a total of 13 pairs of related relationships that need to be calculated through the DTW algorithm. According to the calculation, the alternate points are obtained using the [1, 2, 3, 4, 5] dataset. As mentioned earlier, 3 alternative points are selected for the diffused tracks [1, 2, 3, 4, 5], and these 3 alternative points of the 5 tracks can be calculated based on the DTW algorithm, following the position indicated by the arrows.

As shown in Figure 10, the calculation relationship of the alternative points is indicated by the arrows in Figure 10. Each horizon in [1, 2, 3, 4, 5] has 3 alternative points and calculates their correlation with the adjacent 3 alternative points. The correlation relationship between the alternative points of horizon 1 and horizon 2 can be expressed as the following formula:

$$\varepsilon^{12} = \varepsilon_{\mathrm{i \cdot j}}\ (\mathrm{i} = 1,2,3; \mathrm{j} = 1,2,3) \tag{1}$$

where ε^{12} represents the correlation value between a candidate point in path 1 and a candidate point in path 2, $\varepsilon_{\mathrm{i \cdot j}}$ specifically represents the connection coefficient between two candidate points i and j, where i and j represent a candidate point in path 1 and path 2, respectively. The correlation coefficient of a certain connection path can be represented by Equation (2):

$$\varepsilon 1 = \varepsilon^{12} + \varepsilon^{23} + \varepsilon^{34} + \varepsilon^{45} \tag{2}$$

where $\varepsilon 1$ represents the correlation coefficient of a connecting path. Since there are 3 candidate points in each channel, there are 3 choices. With a total of 5 channels, there are 3^5 possible combinations. One arrow in Figure 9 represents one correlation calculation; a total of 13 correlation values are calculated. Equation (2) represents 4 of the correlation coefficients, and the remaining 9 correlation coefficients are shown in Equations (3)–(5).

$$\varepsilon 2 = \varepsilon^{a1} + \varepsilon^{b2} + \varepsilon^{c3} \tag{3}$$

$$\varepsilon 3 = \varepsilon^{a2} + \varepsilon^{b3} + \varepsilon^{c4} \tag{4}$$

$$\varepsilon 4 = \varepsilon^{a3} + \varepsilon^{b4} + \varepsilon^{c5} \tag{5}$$

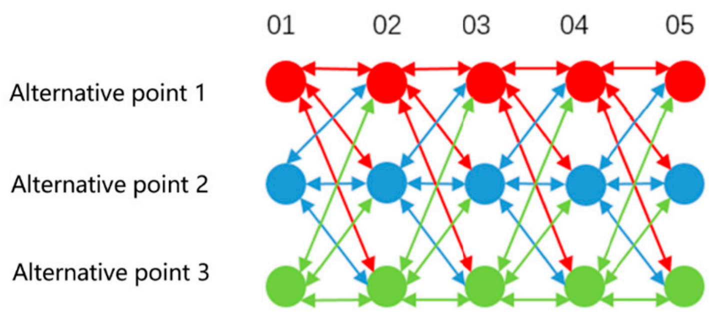

Figure 10. Correlation calculation of alternative points.

The total correlation coefficient can be obtained through the follow formula:

$$\varepsilon = \varepsilon 1 + \varepsilon 2 + \varepsilon 3 + \varepsilon 4 \tag{6}$$

There are 3^5 results for ε, and by sorting and selecting the maximum value of ε, we obtain the corresponding 5 candidate points.

As shown in Figure 11, this is a set of optimal solutions, selecting these 5 optimal points from among 15 candidate points as the diffused horizon points. Only the middle horizon points (i.e., the red points in channel 3) are needed, as shown in Figure 12.

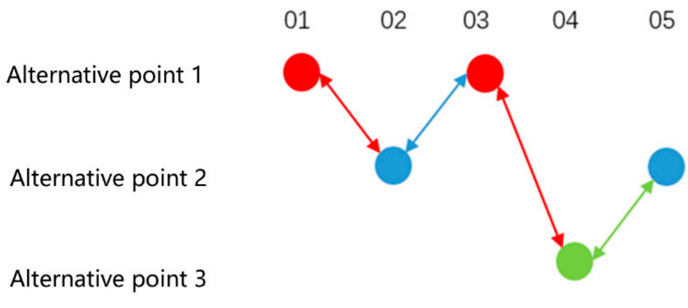

Figure 11. Optimal path.

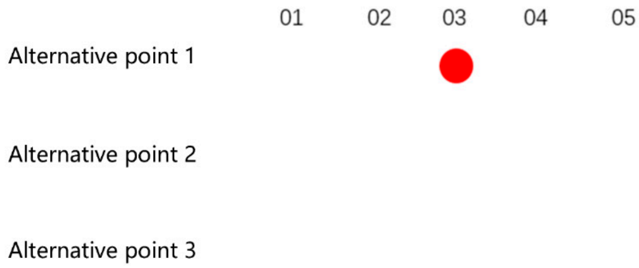

Figure 12. Diffusion point.

Thus, the horizon label θ that is passed is determined at the 3-dimensional spatial position, and the matrix label values of the points shown in Figure 12 are marked as θ, where the labeling is successfully passed. The other labeling information transmission process is the same. The next step is to pass the horizon label θ from seismic channel c to seismic channel 4 (as shown in Figure 8, the arrow direction is the horizon transmission direction), the selection of the window and calculation process remains unchanged, and this process is repeated until it is finished.

To ensure that there is no labeling or horizon mixing when adjacent horizons diffuse, we also need to impose certain diffusion restrictions on the two adjacent horizons.

As shown in Figure 13, the horizon label ω and λ on channel a have the same spatial constraints (+/−2) during the horizon label transfer process from channel a to the outer ring channel 1.

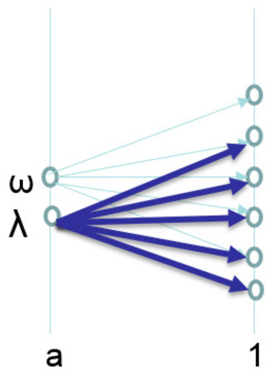

Figure 13. Adjacent horizon diffusion limit.

After the transfer of the ω level on track a is completed, during the transfer of the λ level, we detect the points set below the candidate point of the λ level on track 1, and see if it has already been occupied by the ω level or higher-level labels. If this is the case, the optimal candidate point for this λ level is denied, and the second best among the 3 alternative level points is selected. Repeat the check if all three alternative points do not meet the criteria, and discard the propagation of the λ level on track 1. This process can prevent level crossing.

As discussed above, the situation discussed refers to the case where there is a mapping horizon label on all the data tracks within the inner circle. If a track is missing a mapping label, the transmission window and calculation of the correlation coefficients will have to change.

As shown in Figure 14, this Figure shows two special cases.

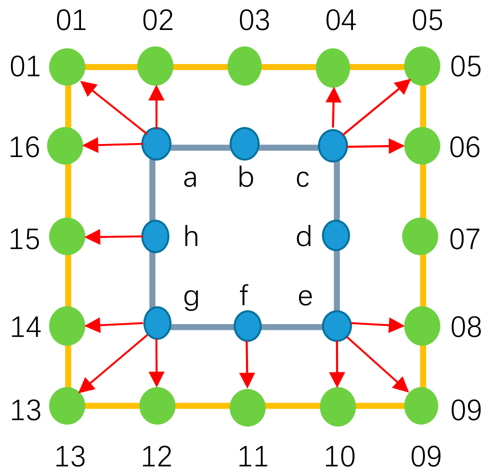

Figure 14. Transmission loss.

When the horizon label θ is missing on tracks b and d, it is not possible to form a diffusion window to transfer the label level to tracks 3 and 7. At the same time, when track a transfers the label to tracks 1 and 2, it also cannot form a diffusion window. The transformation plan is to take the optimal alternative points of tracks 16, 1, and 2 during the horizon level transfer from track a to track 16. The calculation relationship and the selection of the optimal points are shown in Figure 15.

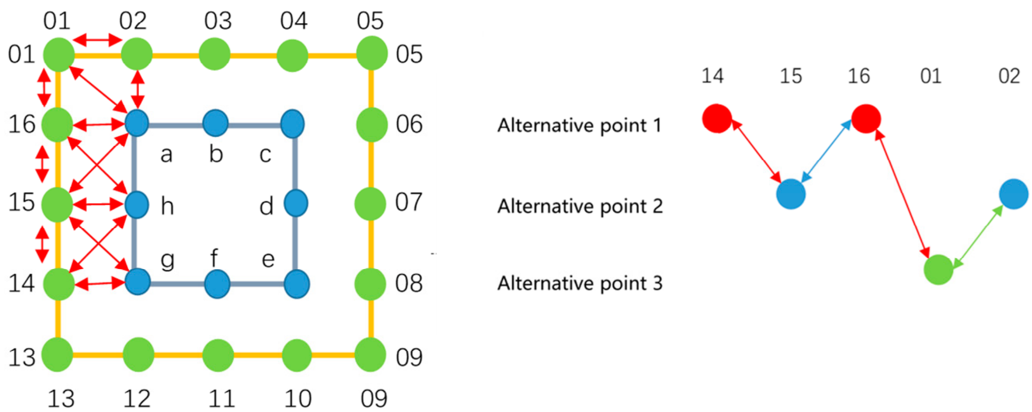

(**a**) (**b**)

Figure 15. Alternative plan. (**a**) Correlation coefficient calculation; (**b**) best selection.

Figure 15a shows the calculation relationship of the correlation coefficient of the diffusion window when the diffusion from trace A to trace 16 occurs, while Figure 15b shows the selected best alternative points. The previously shown method only selects the alternative point 1 of trace 16 as the diffusion point, but due to the lack of horizon mapping on trace B, it is necessary to select the alternative points of trace 16, 1, and 2 as the diffusion points at the same time.

The second special relationship is shown in Figure 15, where both the b and d tracks lack the mapped horizon position θ, and only the middle track c has a horizon position to be transmitted. In this case, the correlation information can be calculated once, and the correlation calculation diagram and the best point selection scheme can be calculated using the following method, as shown in Figure 16.

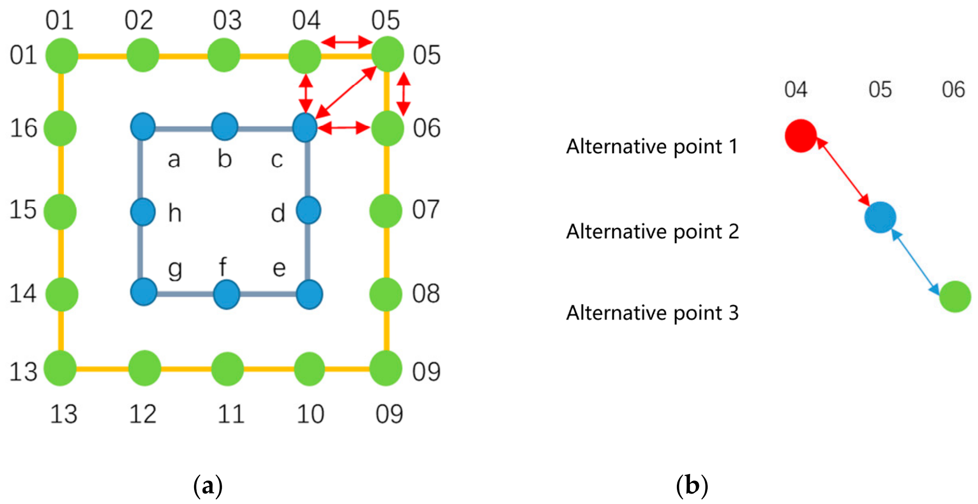

Figure 16. Option 2. (**a**) Correlation coefficient calculation; (**b**) best selection.

The calculation relationship is shown in Figure 16a, only 5 sets of related information need to be calculated and 3 best points need to be selected from 9 candidate points. Then, the horizon position label of c is transferred to 4, 5, and 6, thus completing one horizon-position labeling.

If only single-to-single horizon position transfer is used, such as when there is no horizon position label waiting to be spread between a and c, only the middle line b transfers the horizon position information to 3 lines, and this process can be discarded.

3. Case Analysis

The test area that was selected represented three-dimensional seismic data in the QNand DN regions. The QN three-dimensional work area has two obvious faults, rich sedimentary phenomena, such as horizon superimposition and sharp disappearance in the data body, and a steep structure at the edge of the work area; its size is 550 × 401 × 401. The DN work area has a back-dipping structure overall, with a steep structure, many extreme values, and poor continuity for the same-phase axis; its size is 280 × 251 × 251.

Figures 17–21 show the results of the automatic horizon tracking in the DN region using 3D seismic data. Figure 17 is the thinned horizon position section of inline 120, Figure 18 is the thinned horizon position section of xline 145, and the section position is shown in Figure 19. Figure 19 is a three-dimensional display of horizon D1 (the red horizon line in the section). The tracking results show that the method can ensure the continuity of the tracked horizon position in data with more blurred common-phase axes, and the same inclination can be maintained for the horizon position in data with a large horizon dip. Overall, the algorithm achieved good tracking results in the DN data.

Figures 20–22 are the results of automatic horizon tracking for the Qinnan 3D seismic data, Figure 20 is a 2D display of the inline cross-section, Figure 21 is a 2D display of the xline cross-section, and Figure 22 is a 3D display of the Q1 horizon (the red horizon line in the cross-section). As can be seen from the tracking results, the method in this paper can automatically terminate the horizon at the overlapped and sharp-extinct areas, effectively restoring the horizon structure, and is helpful for identifying rock horizon traps. When the fault spacing is small, the method can achieve good automatic tracking over faults.

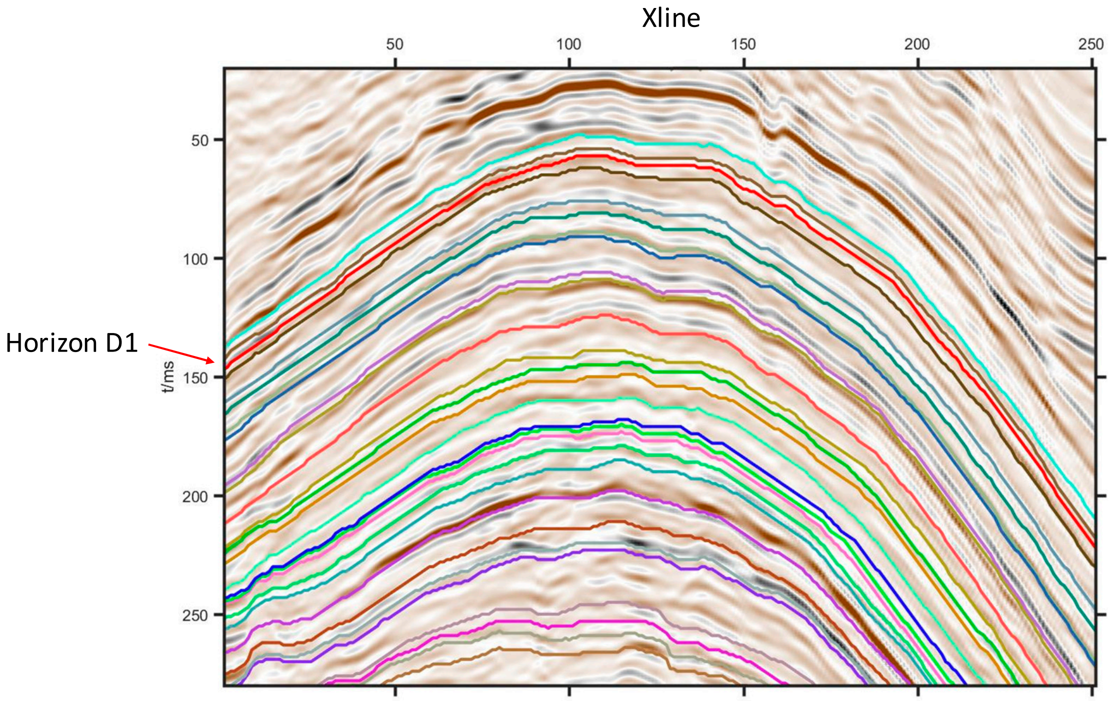

Figure 17. Automatic 3D seismic horizon-tracking results based on global corrugated diffusion in the DN work area (inline120).

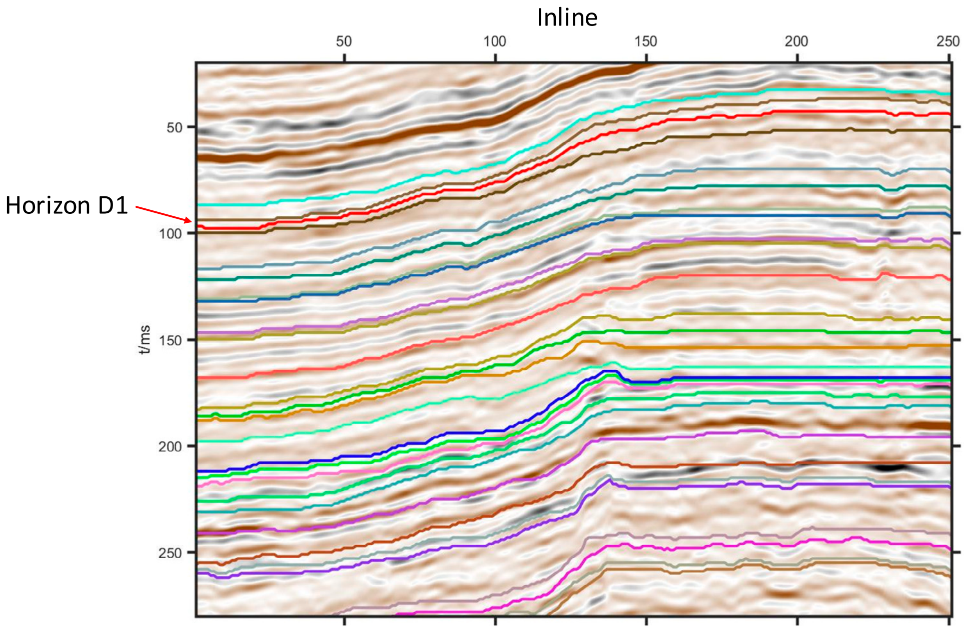

Figure 18. Automatic 3D seismic horizon-tracking results based on global corrugated diffusion in the DN work area (xline145).

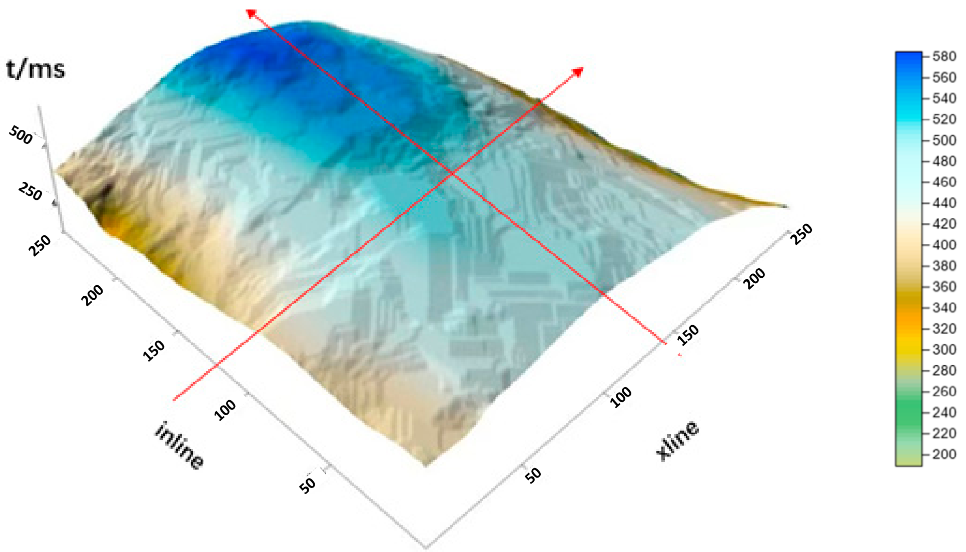

Figure 19. Stereoscopic display of 3D seismic automatic horizon-tracking results for horizon D1.

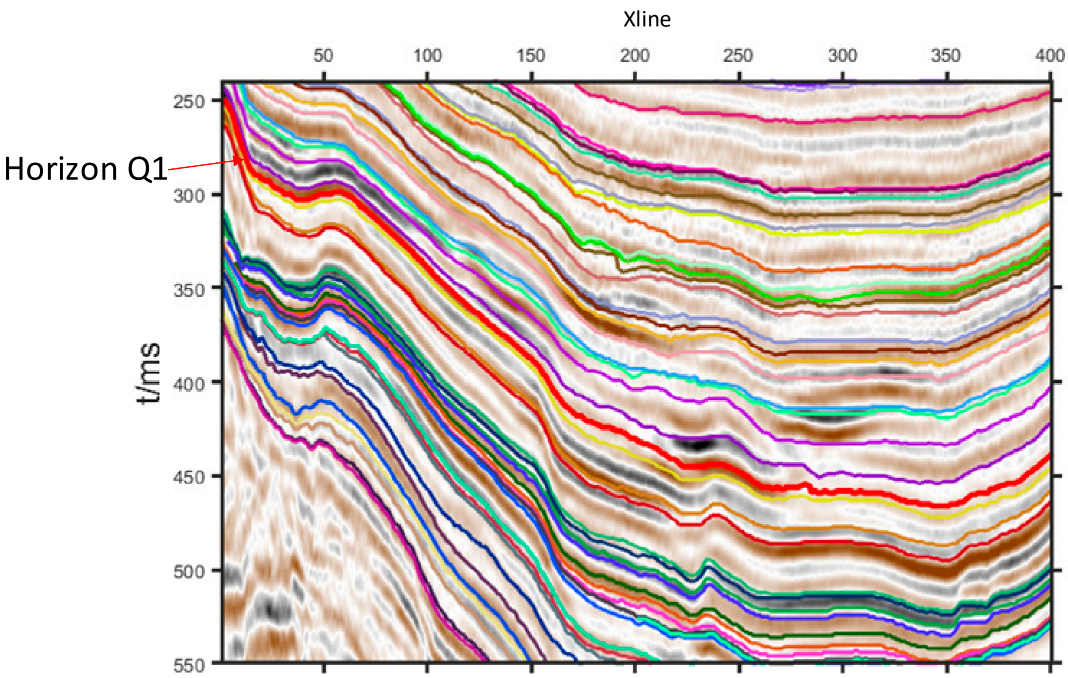

Figure 20. Automatic 3D seismic horizon-tracking results based on global ripple diffusion in the Qinan area (inline170).

The tracking results show that (1) the seismic phases in the data volume are effectively tracked along the common axis, and the traced horizons reflect the actual stratum trend, accurately describing the stratum structure, and there is no horizon phenomenon; (2) the horizon-tracking results well reflect special sedimentary phenomena, such as foreset, as well as the original stratum contact relationships, such as overlying, underlying, stratum sharp dying, etc.; (3) automatic tracking across the faults is well achieved; (4) the horizon tracking results well preserve the structural details.

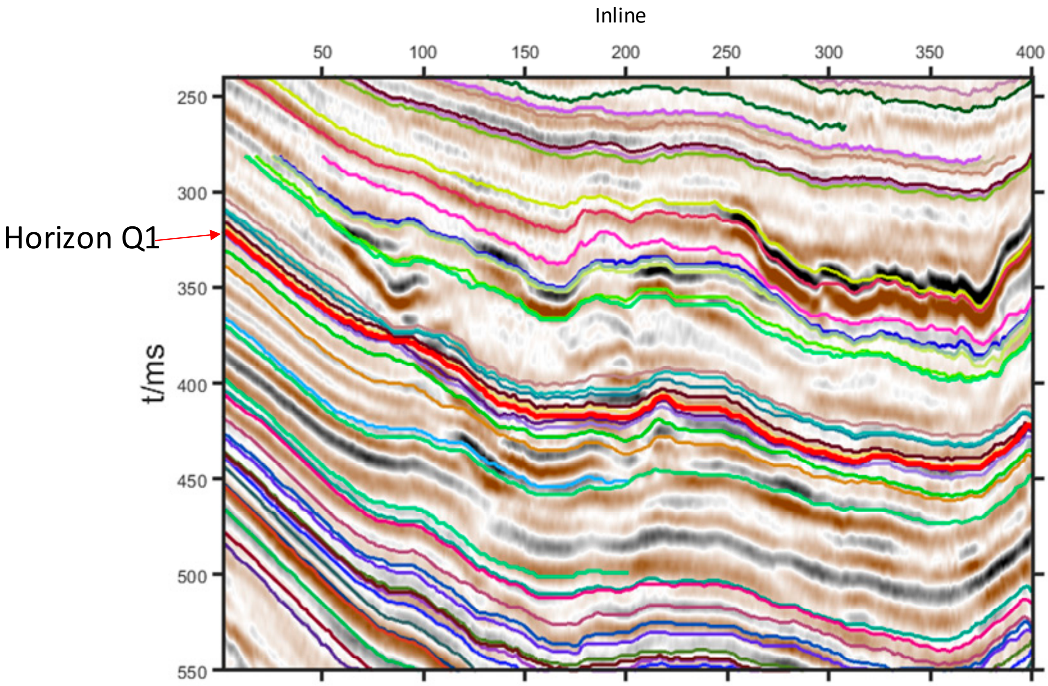

Figure 21. Automatic 3D seismic horizon-tracking results based on global ripple diffusion in the Qinan area (xline175).

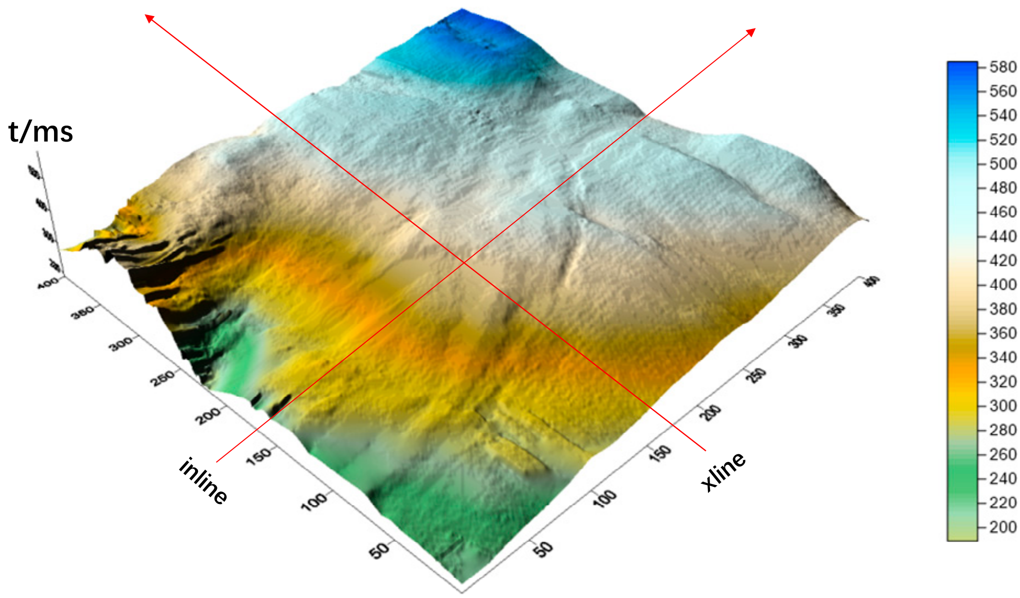

Figure 22. Stereoscopic display of 3D seismic automatic horizon-tracking results for horizon Q1.

Limitations of the Algorithm

(1) Scene restrictions: Due to the DTW algorithm (based on correlation calculations) being the main algorithm in this paper, representing the assumption that data points from the same horizon have similar waveforms that are reflected in the correlation coefficients, the correlation coefficients are relatively high. When calculating similarity, it is necessary to scan a certain search window for data-sampling points as potential horizon candidates. However, if there are faults with large gaps, this method cannot scan the corresponding horizon points since the search window cannot be too large to avoid the problem of excessive calculation complexity due to frequent similarity calculation. Therefore, when

there are faults with large gaps, the algorithm in this paper is limited in its application and needs to be further developed and improved in the future.

(2) Parameter sensitivity: As mentioned above, the algorithm relies on the calculation of similarities between the same horizon, and it is well known that the calculation of similarities of waveforms depends on the parameters. This is also a major flaw in the calculation of similarity, such as the length of the correlation window and the search range, which will result in changes in the similarity value and affect the horizon-tracking result. Fixed correlation window selection cannot adapt to data changes, such as longer or shorter waveform periods. Ideally, different window lengths should be selected to achieve the best correlation window length. However, the data dynamics show complex changes, and it is difficult to form a clear relationship between the window width and data dynamics, so it is difficult to dynamically determine the correlation window.

(3) Time complexity: Due to the innovative use of the DTW algorithm based on wave diffusion, this algorithm requires a diffusion calculation regarding all the surrounding points for the diffusion of the seed points, meaning that it requires more correlation calculations when compared to traditional methods, and the calculation complexity of correlation is also relatively high, resulting in a greater time calculation complexity for this algorithm. Of course, with the advancement of computer hardware technology, the introduction of highly parallel computing and GPU devices will mitigate this defect to some extent.

4. Conclusions

This paper presents a method for calculating and reconstructing 3D seismic data horizon models based on the correlation coefficients between seismic data and 3D grids. Firstly, the correlation coefficients between several neighboring seismic traces were estimated, the best correlation linkage path was extracted through DTW, and then the seismic horizon seed points were expanded and linked; the global correlation coefficients were obtained by adjusting the local linkage paths. Finally, the optimal seismic model for horizon interpretation was obtained through ripple-style global diffusion. This method has good seismic horizon interpretation effects, and the core algorithm can be used to combine with traditional horizon-tracking algorithms and improve their performance. The example shows that the strata tracked by this method better reflect the original stratigraphic endowment and stratum-contact relationship, retain their structural details, cumulatively reflect the structural shape, and realize the automatic tracking between faults. In the future, the algorithm model used in this paper can be further improved, and more applications can be realized for various 3D seismic data.

Author Contributions: Methodology, M.S. and S.C.; Software, F.Q.; Validation, C.Y.; Writing–review & editing, X.C. All authors have read and agreed to the published version of the manuscript.

Funding: China National Petroleum Corporation's Major Technology R&D Project "Key Technologies for Fine Characterization of Lithostratigraphic Trap and Seismic Sedimentology Research" (Project No.: 2021DJ0403).

Institutional Review Board Statement: Not applicable.

Informed Consent Statement: Not applicable.

Data Availability Statement: Not applicable.

Conflicts of Interest: The authors declare no conflict of interest.

References

1. Hoyes, J.; Cheret, T. A review of global interpretation methods for automated 3D horizon picking. *Lead. Edge* **2011**, *30*, 38–47. [CrossRef]
2. Wu, X.; Hale, D. Extracting horizons and sequence boundaries from 3D seismic images. In Proceedings of the Houston 2013 Annual Meeting, Houston, TX, USA, 2–5 May 2013; pp. 1440–1445. [CrossRef]

3. Wu, W.; Tan, S.; Wang, S.; Yu, H. Automatic horizon tracking method based on waveform classification. In Proceedings of the 2020 International Geophysical Conference in Nanjing, Nanjing, China, 13–16 September 2020; Volume 4.
4. Pauget, F.; Lacaze, S.; Valding, T. A global approach in seismic interpretation based on cost function minimization. In *SEG Technical Program Expanded Abstracts 2009*; SEG Library: Hong Kong, China, 2009.
5. de Groot, P.; Huck, A.; de Bruin, G.; Hemstra, N.; Bedford, J. The horizon cube: A step change in seismic interpretation. *Lead. Edge* **2010**, *29*, 1048–1055. [CrossRef]
6. Stark, T.J. Relative geologic time (age) volumes—Relating every seismic sample to a geologically reasonable horizon. *Lead. Edge* **2004**, *23*, 928. [CrossRef]
7. Stark, T.J. Unwrapping instantaneous phase to generate a relative geologic time volume. In *SEG Technical Program Expanded Abstracts 2003*; Society of Exploration Geophysicists: Houston, TX, USA, 2003; pp. 1707–1710.
8. Wu, X.; Zhong, G. Generating a relative geologic time volume by 3D graph-cut phase unwrapping method with horizon and unconformity constraints. *Geophysics* **2012**, *77*, 21. [CrossRef]
9. Geng, Z.; Wu, X.; Shi, Y.; Fomel, S. Relative geologic time estimation using a deep convolutional neural network. In *SEG Technical Program Expanded Abstracts 2019*; SEG Library: Hong Kong, China, 2019.
10. Harrigan, E.; Kroh, J.R.; Sandham, W.A.; Durran, T.S. Seismic horizon picking using an artificial neural network. In Proceedings of the IEEE International Conference on Acoustics, Speech, and Signal Processing, Singapore, 22–27 May 2022; IEEE Computer Society: Washington, DC, USA, 1992; Volume 3, pp. 105–108.
11. Borgos, H.G.; Skov, T.; Sønneland, L. Automated Structural Interpretation through Classification of Seismic Horizons. In *Mathematical Methods and Modelling in Hydrocarbon Exploration and Production*; Springer: Berlin/Heidelberg, Germany, 2005.
12. Tschannen, V.; Delescluse, M.; Ettrich, N.; Keuper, J. Extracting horizon surfaces from 3D seismic data using deep learning. *Geophysics* **2020**, *85*, N17–N26. [CrossRef]
13. Shi, Y.; Wu, X.; Fomel, S. Waveform embedding: Automatic horizon picking with unsupervised deep learning. *Geophysics* **2020**, *85*, WA67–WA76. [CrossRef]
14. Lv, X.; Cao, J.; Hu, J.; lu, Y.; He, Y. Seismic horizon automatic tracking based on dynamic time warping. In Proceedings of the CPS/SEG Beijing 2018 International Geophysical Conference & Exposition Electronic Papers, Beijing, China, 24–27 April 2018; Volume 5.
15. Jin, S.; Chen, S.; Wei, J.; Li, X.Y. Automatic seismic event tracking using a dynamic time warping algorithm. *J. Geophys. Eng.* **2017**, *14*, 1138–1149. [CrossRef]
16. Hale, D. Dynamic warping of seismic images. *Geophysics* **2013**, *78*, S105–S115. [CrossRef]
17. Berndt, D.J.; Clifford, J. Using dynamic time warping to find patterns in time series. In Proceedings of the 3rd International Conference on Knowledge Discovery and Data Mining, Seattle, WA, USA, 31 July–1 August 1994; Volume 10, pp. 359–370.